THE JOURNAL OF PHYSICAL CHEMISTRY C

Article

pubs.acs.org/JPCC

Control of Photoactivity over Polycrystalline Anatase TiO_2 Thin Films via Surface Potential

S. W. Daniel Ong,[‡] Jianyi Lin,[§] and Edmund G. Seebauer*[,†]

[†]Department of Chemical and Biomolecular Engineering, University of Illinois at Urbana−Champaign, Urbana, Illinois 61801, United States

[‡]Institute of Chemical and Engineering Sciences, Jurong Island, Singapore 627833, Singapore

[§]Energy Research Institute @ Nanyang Technological University, Singapore 637141, Singapore

ABSTRACT: The utility of thin-film TiO_2 for photocatalysis would be greatly improved if the spatial variation of the electronic band edges near the surface could be engineered a priori to control the current of photogenerated minority carriers. The present work demonstrates such a concept. In particular, remote oxygen plasma treatment of polycrystalline anatase TiO_2 with specified majority carrier concentration is employed in the test case of methylene blue photodegradation. The photoreaction rate varies by up to 35% in concert with a 0.4 eV change in built-in surface potential measured by photoelectron spectroscopy. The correlation between these changes agrees quantitatively with a photodiode−photocurrent model. The plasma treatment affects concentration of charged native defects within the first few atomic layers of the surface, most likely by lowering the concentration of oxygen vacancies within surface crystallites. In tandem, the position in the deep bulk is controlled via engineering the defect concentration at grain boundaries, thus illustrating the coordinated use of multiple defect engineering practices in polycrystalline material to accomplish quantitative manipulation of band bending and corresponding photocurrent.

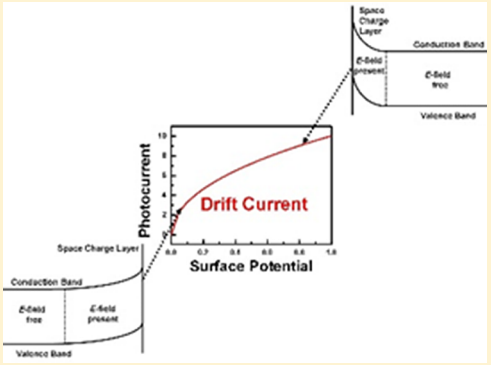

INTRODUCTION

Thin-film semiconducting photocatalysts find applications in self-cleaning windows/other weather-exposed surfaces,[1,2] and in antimicrobial[3,4]/antifouling coatings.[5,6] Moreover, the anatase form of TiO_2 is a promising catalyst for water purification and advanced oxidation processes (AOP) because of its low cost, nontoxicity, and capacity for degrading recalcitrant dyes, pesticides, and volatile organic compounds in wastewater. Although suspensions of particles may be used in photocatalytic systems, catalyst separation and recovery impose additional cost. An alternative is to immobilize the catalyst on a support, with the trade-off being a reduction in the active area. This decrease in area could be compensated, however, if minority photocarriers could be driven more efficiently to the surface.[7] Manipulation of the direction and magnitude of photocurrent is commonplace in conventional optoelectronics, mostly via semiconductor band-engineering techniques that employ heterostructures with background carrier concentrations via manipulation of the concentrations and spatial distributions of substitutional and native point defects. Rarely is a free surface involved, however, which in photocatalysis provides both the locus of chemical activity and an additional avenue to accomplish band engineering. In particular, surface photocurrent may be driven through manipulation[8] of near-surface electric fields via the magnitude and sign of the surface potential, V_S, which in principle may be manipulated in turn via the controlled placement of charged point defects on or very near the surface. This form of defect engineering, which translates into band engineering for photocurrent control, has been demonstrated in conventional microelectronics applications[9−12] but not in thin-film photocatalysis. The present work demonstrates such a concept through the use of remote oxygen plasma treatment of polycrystalline anatase TiO_2 in the case of methylene blue (MB) photodegradation.

The unambiguous demonstration of this idea stems partly from the complexities of polycrystalline wide band gap semiconductors with electrically active grain boundaries and partly from the difficulty in controlling background carrier concentration reliably. This latter difficulty is especially pronounced because of a dearth of dopants having shallow donor or acceptor levels,[13] effects of poorly controlled concentrations of native point defects serving as donors or acceptors,[14,15] and effects of charged defects at grain boundaries.[16] Nevertheless, recent work in this laboratory has demonstrated that suitably prepared polycrystalline anatase effectively acts as a uniform medium with a donor concentration N_D that varies with the engineered concentration of grain boundary defects.[13,16,17] N_D scales inversely with film thickness because of a progressive decrease in grain boundary area that is available for accumulating defects with excess

Received: September 23, 2015
Revised: November 5, 2015
Published: November 9, 2015

ACS Publications © 2015 American Chemical Society

DOI: 10.1021/acs.jpcc.5b09272
J. Phys. Chem. C 2015, 119, 27060−27071

charge.[13,16,17] This effect felicitously avoids the need for extrinsic dopants, which engender complications that could affect reaction rates such as segregation to the surface. The width of the space charge layer (SCL) near the surface varies with N_D, and a wider SCL leads to a larger volume from which generated photocarriers can be swept to the surface to increase the photocurrent.

The present work focuses on a different form of defect engineering, in which the spatial distribution of charged defects is controlled by employing remote oxygen plasma treatment to change the concentration of charged native defects within the first few atomic layers of the surface, most likely by lowering the concentration of oxygen vacancies within surface crystallites. The literature on MB photodegradation by TiO_2 is voluminous,[18−28] making this reaction a useful, well-characterized test case for unambiguously demonstrating phenomena that result from band manipulation.

METHODS

Photocurrent Model. A key parameter in band engineering is the width of the SCL, the behavior of which is governed by the equation[29]

$$W = \sqrt{\frac{2\varepsilon\varepsilon_0}{q}\frac{V_S}{N_D}} \quad (1)$$

where W is the SCL width, ε the dielectric constant of the semiconductor, ε_0 the permittivity of free space, q the electronic charge, V_S the surface potential, and N_D the (spatially uniform) donor carrier concentration. Within the SCL, the built-in electric field can play a crucial role in the transport of charge carriers to and from the surface of the semiconducting material, effectively influencing the type and number of charges that get to participate in surface reactions. We had previously reported the change in photoactivity of a polycrystalline anatase TiO_2 photocatalyst based on variations in N_D, where we obtained good adherence of actual rate improvement with that predicted by a photocurrent model based on the photodiode and governed by the equation[30]

$$J_{pc} = J_0(1 - e^{-\alpha W}) + J_0\left(\frac{\alpha L_p}{1 + \alpha L_p}e^{-\alpha W}\right) \quad (2)$$

where J_{pc} is the minority charge photocurrent, J_0 the photocurrent if all incident light stimulated electron−hole pairs (EHPs), α the absorption constant, and L_p the minority charge diffusion length. The first term in parentheses represents the drift component of the photocurrent while the second term represents the diffusion component. In contrast to our previous work where N_D was varied to effect changes to the photocurrent, we now vary V_S to test the photocurrent model's correlation with photocatalytic activity.

The methodology employed in this study makes use of normalized changes with respect to reaction rate measurements made on 300 nm films. There is good reason to believe that photocarriers generated within the SCL are effectively promoted to the surface. There are reports in the literature that the lifetime of electron−hole pairs (EHPs) in TiO_2 is in the vicinity of 10^{-8} s,[31,32] whereas the time taken to sweep the EHPs out of an SCL of 50 nm with a surface potential of 0.1 eV can be calculated to be on the order of 10^{-12} s. If we assume a typical donor charge concentration of $\sim 10^{17}$ cm^{-3} for TiO_2, increasing the surface potential from 0 to 1 eV results in the increase of J_{pc} from 1 to 10 μA cm^{-2}. This represents an increase by a factor of about 10 and translates to an extra $\sim 10^{12}$ cm^{-3} s^{-1} of minority charges migrating to the surface. Although not all charges promoted to the surface this way will get to participate in a surface reaction, we think it reasonable that the catalytic turnover frequency (TOF) will scale by the same factor as the photocurrent.

Wilson and Idriss investigated the reconstructed surfaces of the $TiO_2(001)$ − {011} and {114} faceted surfaces and the effect they had on the photoreaction of acetic acid.[33] They argued that changes in reactivity are due to the changes in the electric field in the SCL caused by the last-layer atomic arrangement of the surface. The surface potentials and SCL width for the two facets were estimated from the quantum yield of acetic acid decomposition, with V_S calculated to be 0.18 and 0.023 V for the {011} and {114} facets, respectively, while their SCL widths were estimated at 18.2 and 6.6 nm, respectively. The quantum yield of the {110} facet over that of the {114} facet was about 2.5 times. Using our model with key parameters of donor concentration as $N_D = 1 \times 10^{17}$ cm^{-3} and dielectric constant of $\varepsilon_r = 170$ used by those authors, together with other nonadjustable parameters like α and L_p, the predicted improvement is 2.3 times, as shown in Figure 1. The increase

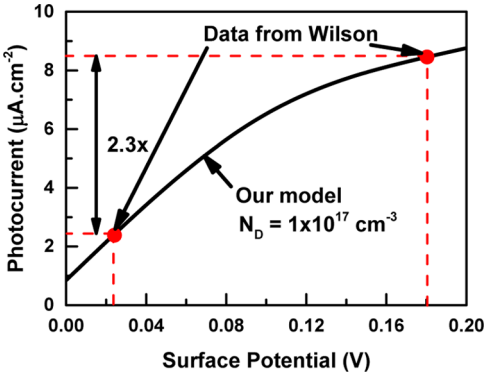

Figure 1. Photocatalytic rate data taken from ref 33 matched to the photocurrent trend from our model. The model predicts an improvement of 2.3 times. The experimental data shows an improvement of 2.5 times.

in apparent quantum yield was measured by the authors to be a factor of 2.5, close to the estimated improvement in photocurrent (or equivalently, quantum yield) by our photocurrent model. This result indicates the applicability of the current model to their system and reinforces the case that surface fields affecting charge-transfer kinetics across the surface could and should play a dominant role.

Figure 2 shows the trend in drift and diffusion components of the photocurrent within a range of 1 eV for surface potential. We see that improvements to the reaction rates will come mainly from the drift component of the photocurrent. This should come as no surprise as band engineering seeks to control the preferential flow of electrons or holes to the catalyst surface by manipulating the built-in field in the SCL. For flat bands where there is no electric field, we can expect hole promotion to the surface to be diffusion-controlled.

During the development of the photocurrent model, a number of assumptions were made. We assumed that changes in turnover frequency (TOF) are proportional to changes in photocurrent and that the donor concentration (primarily in the form of native defects at grain boundaries[13]) throughout

DOI: 10.1021/acs.jpcc.5b09272
J. Phys. Chem. C 2015, 119, 27060−27071

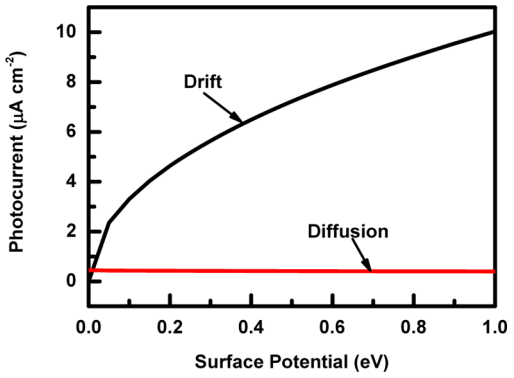

Figure 2. Variation of photocurrent with surface potential. The expected improvement over flatband conditions is about ten times over a range of 1 eV. Note that the drift current plays the dominant role compared to the diffusion current.

the bulk is uniform. The polycrystalline films we used were also assumed to act as uniform media. What comes as surprising then is the effectiveness of this formulation in predicting rate changes by considering the flux of minority charge carriers to the surface, demonstrating the importance of the near-surface field in the optimization of surface photocatalytic reactions.

Experimental Details. *Photoreaction Rate Measurements.* The photoreaction of aqueous methylene blue (MB) over TiO_2 anatase thin film was measured on a setup comprising a reaction vessel, ultraviolet (UV) light source and a UV−visible (UV−vis) spectrometer (UV-3600 from Shimadzu). The UV light source used was the UVP Blak-Ray B-100 high-intensity UV lamp which houses a 100 W Sylvania H44GS-100 M mercury spot light bulb that strongly emits in the 365 nm UV wavelength.[2]

Pure methylene blue (MB) hydrate (75%) was obtained from ACROS ORGANICS (formula weight of 319.85 g mol^{-1}). A stock solution of 0.8 mM MB was prepared using deionized water. In each photodegradation experiment a solution of 5 μM MB was obtained by diluting 0.625 mL of 0.8 mM solution in a 100 mL volumetric flask with deionized water.

The photoreaction was carried out batchwise with an initial MB concentration of 5 μM over 100 min of UV irradiation at pH 6.4. The concentration of the solution after the UV irradiation was determined using a UV−vis instrument from Shimadzu and used to calculate the pseudo-first-order rate equation given by[19−21,34]

$$r = k_r C_{MB} \quad (3)$$

where r is the reaction rate, k_r the apparent rate constant, and C_{MB} the concentration of MB.

Remote Oxygen Plasma Treatment of TiO_2. Remote oxygen plasma treatment was performed in a stainless steel chamber 12 in. in diameter with a sample holder 8 in. in diameter. The plasma was generated by applying an RF (13.56 MHz) between two electrodes and is composed of electrons, charged ions, and neutral molecules. The thin film was placed on a platform in the center of the chamber, which acted as the cathode. Oxygen was fed into the chamber via a mass flow controller set at 20 sccm. The plasma operates on the basis of a simplified ion space-charge-limited model[35] where the plasma ion energy and the ion flux are related to the sheath voltage as

$$E_{ion} \propto V^{4/5} P_O^{-1/2} \quad (4)$$

$$n_{ion} \propto V P_O^{3/4} \quad (5)$$

where E_{ion} is the plasma ion energy, n_{ion} the ion flux, V the sheath voltage, and P_O the oxygen pressure. Throughout the treatment, the RF power used was 50 W and chamber pressure was kept at 100 Pa. Treatment times were varied from 10 to 90 min. A bias of 1.1 kV was set up via a mesh placed above the films to prevent the impingement of energetic positive ions onto the surface that might damage the film.

Other experimental methods have been described previously.[8,16] In brief, films were grown via atomic layer deposition (ALD) on commercial n-type Si(100) (Sb, 0.013 Ω cm resistivity, 2 cm × 2 cm) at 400 °C. The precursors were $Ti(OCH(CH_3)_2)_4$ (TTIP, Strem Chemicals Inc., 98%) and H_2O (deionized, no further purification), with N_2 (SJ Smith, 99.999%) serving as the carrier gas. A full growth cycle consisted of a TTIP pulse (8 s), N_2 purge (10 s), H_2O pulse (8 s), and another N_2 purge (10 s). Film thickness was determined by ellipsometry. Annealing at 550 °C for 24 h was performed to crystallize the anatase phase.

Characterization. X-ray photoelectron spectroscopy (XPS) and ultraviolet photoelectron spectroscopy (UPS) were performed in a Thermo VG Scientific ESCALAB 250 Photoelectron Spectrometer with an ultrahigh vacuum system (base pressure ~10^{-10} mbar), using a monochromated X-ray source (Al Kα at 1486.6 eV) and helium discharge lamp, respectively. The work function of the instrument and the energy scale were calibrated using a clean Ni reference. Brunauer−Emmett−Teller (BET) surface area was studied in Micromeritics ASAP 2420. X-ray diffraction (XRD) patterns were obtained at room temperature with a high-resolution Bruker D8 diffractometer from Bruker AXS operated at 45 kV and 40 mA with a Cu Kα I primary X-ray beam (λ = 1.5406 Å).

RESULTS

Plasma Treatment. Oxygen plasma treatment is used frequently in industry as well as in research. In cases where the area of interest is the material surface, plasmas may be set up so that the impinging ions do not damage the bulk material. This is commonly seen in surface cleaning[36] and the ashing of photoresists, as well as in the surface modification of TiO_2 to change their performance profile, such as improving the efficiency of dye-sensitized solar cells[37,38] and changing the responsiveness of photodetectors.[39] There are also cases where ion bombardment of the material is desired, such as in extending the bandwidth of light-response into the visible region for photocatalysis.[40] Although it can be assumed that surface modification has occurred via plasma treatment, the mechanism behind the reported changes was either unexplored or commonly attributed to the increase in oxide to suboxide ratios after treatment with oxygen. We believe that in the present case the changes could be directly attributed to variations in the surface potential and that it is possible to "re-pin" the Fermi level through the action of oxygen plasma treatment. Microstructural changes to the TiO_2 films after plasma treatment were precluded by performing the treatments at room temperature.

To correlate our result to the degree of band bending, we precluded contributions from other sources, allowing us to establish with confidence that changes in MB degradation rates were caused by affecting the near-surface electric field responsible for electron−hole separation and in our case, the promotion of photogenerated holes to the catalyst surface. To

DOI: 10.1021/acs.jpcc.5b09272
J. Phys. Chem. C 2015, 119, 27060−27071

date, we believe no reports have attempted a coherent synthesis of experimental data on surface field changes and photocatalytic rate changes, bolstered by a simple, yet predictive photocurrent model. We think a fuller picture can be obtained when these elements are brought together to offer a richer, deeper insight into the optimization of surface processes.

Methylene Blue Degradation Rate. Figure 3 shows the percentage change in initial rate of MB degradation with various surface treatment times. The treatment times range from 10 to 90 min with an obvious decrease in initial rate with increasing length of treatment time. Successive runs on a single piece of film show robustness and repeatability of the treatment protocol, as shown in Figure 4. The film, treated with a positive bias to shield the film from impinging cations, showed a decrease in MB degradation rate and retained this diminished activity even after exposure to water and ambient air. Successive treatment for 20 min with bias served to decrease the rate further in a nearly linear fashion for up to about 40 min of treatment time before showing signs of reaching a minimum near 60 min of treatment. Treating the film for as short a time as 30 s without the use of bias caused the MB degradation to revert to the rates before any oxygen plasma treatment, and subsequent treatment of the film with bias for a whole 60 min caused a decline in the film's photoactivity similar in magnitude to that of three consecutive 20 min treatments, illustrating the cumulative and irreversible nature of these alterations to atmospheric and water exposure.

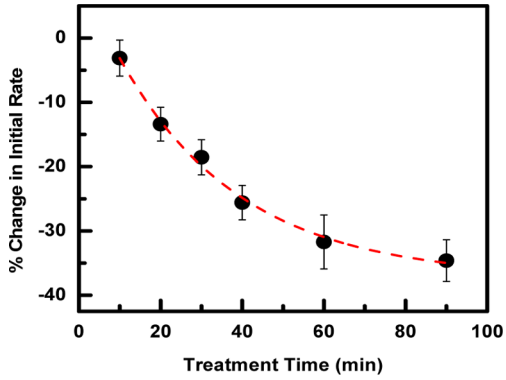

Figure 3. Percentage change in initial rate versus treatment time. (The line is meant to guide the eye.) The trend is one of decreasing initial rate with plasma treatment time, stabilizing near the 60 min mark. Changes were calculated by comparing the initial rates after treatment with the average of initial rates before treatment. Errors are standard errors of coefficient from regression analysis.

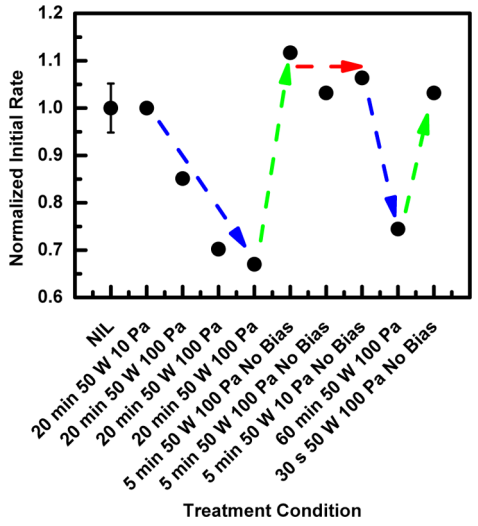

Figure 4. Graph showing successive runs on a single piece of film. The graph is divided into various regions. Starting from the left, there is no change in the initial rate when the film was treated for 20 min at 50 W input power and 10 Pa O_2. When the O_2 pressure was increased from 10 to 100 Pa, successive treatment with a positive bias decreased the photoactivity of the film. Treatment of the film without bias caused the photoactivity to revert to that before any treatment, and a subsequent treatment of 60 min with bias indicates a similar drop in photoactivity as three consecutive 20 min treatments. Because the films were exposed to water and ambient air after each 20 min treatment, it is reasonable to believe that any change to the film caused by treatment is irreversible under normal conditions.

Film Composition and Phase Identification. Figure 5a shows the X-ray photoelectron spectroscopy survey scan of a 300 nm thin-film sample. The identity of the spectrum is matched with that of TiO_2, where clear and strong peaks for Ti 2p, O 1s, and C 1s can be observed. The X-ray diffraction spectra for the 300 nm films are shown in Figure 5b. The spectra are matched to the anatase phase of TiO_2 and show a predominance of (101) facet planes.

Scanning electron microscopy (SEM) was used to compare the microstructure of the films before and after plasma treatment, as shown in Figure 6. No noticeable change to the surface was observed after treatment, allowing us to preclude contributions from microstructure to changes in reaction rate.

Surface Oxidation State and Binding Energy Shift. Figure 7 shows the C 1s XPS peak. The main peak at 284.6 eV is attributed to graphitic carbon and is used as a reference for the other peak positions. Two other C 1s peaks at higher binding energy can be identified as C−O and O═C−OH species, respectively.[41−45] The changes in C−O and O═C−OH species before and after treatment are unremarkable and lead us to conclude that changes to the carbon content on the film surface are insignificant. Figure 8a shows the Ti 2p XPS peaks before and after the oxygen plasma surface treatment are compared, showing no evidence of any suboxide materials present either before or after treatment. Figure 8b shows the O 1s XPS peaks before and after the surface treatment. The O 1s peaks at higher binding energy can be attributed to surface hydroxyl species, which decrease in intensity upon the oxygen plasma treatment.[46−49]

The XPS O-to-Ti ratio was found to change after the surface treatment, as shown in Figure 9. No obvious trend with treatment time could be perceived, although the change in O 1s/Ti 2p is consistently positive. No clear trend with treatment time could be perceived, although the ratio change is consistently positive. This implies that the O-to-Ti ratio has increased by an average value of 2.5% ± 1, which is consistent with mild surface oxidation of the film surface without a significant change in surface stoichiometry.

XPS O 1s and Ti 2p peaks in Figure 8 were both found to shift toward higher binding energy upon the remote oxygen plasma treatment. Careful analysis revealed that this concomitant O 1s and Ti 2p peak shift toward higher binding energy increases with duration of treatment time, as shown in Figure 10. This indicates a relaxation of the surface band bending, leading to a decrease in surface field strength, in turn affecting the rate of photohole promotion to the film surface. The Ti 2p peaks consistently shifted more than the O 1s peaks by ∼0.1 eV. This could be explained by a relative peak shift of the O 1s

DOI: 10.1021/acs.jpcc.5b09272
J. Phys. Chem. C 2015, 119, 27060−27071

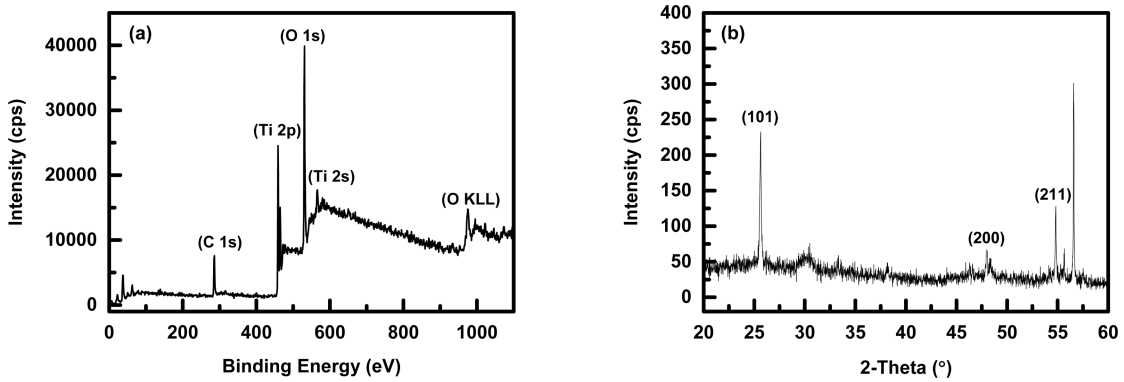

Figure 5. (a) XPS survey scan of the anatase TiO_2 thin film. The binding energy was aligned using the C 1s graphitic carbon peak at 284.6 eV. One can clearly make out the Ti 2p and O 1s peaks identified with TiO_2. (b) XRD pattern for the 300 nm films. The dominant surface plane is (101) with its intensity increasing with film thickness. The phase of the TiO_2 is matched to anatase, and the particle size is estimated at ∼50 nm using the Scherrer equation.

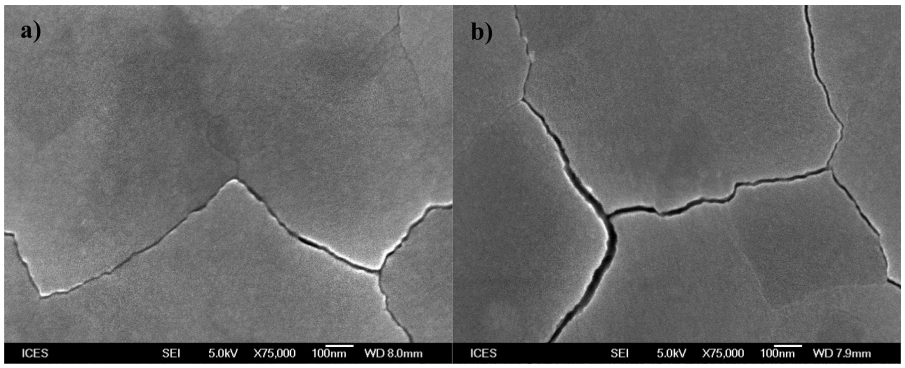

Figure 6. Typical SEM micrographs of the TiO_2 anatase surface (a) before plasma treatment and (b) after plasma treatment at 50 W input power and 100 Pa O_2 for 60 min. No noticeable changes to the surface microstructure of the film were observed.

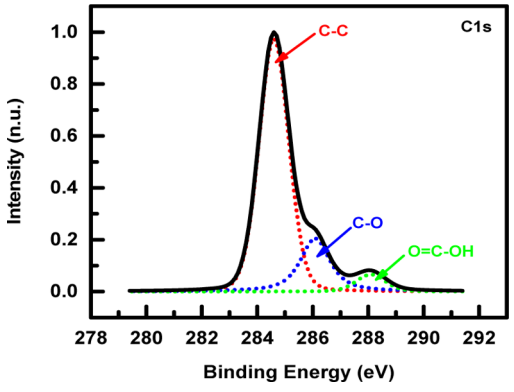

Figure 7. C 1s XPS peak synthesis. The carbon peaks have been identified as having a main graphitic peak at 284.6 eV and two smaller peaks, namely, that associated with C−O and carbonyl, at higher binding energy.[41−45]

and Ti 2p peaks occurring together with their shift to higher binding energy. These shifts confirm the more quantitative determination of V_S via ultraviolet photoelectron spectroscopy, which is more accurate.

Changes in Work Function. The surface Fermi level was measured via UPS by referencing the valence band edge of TiO_2 with the Fermi edge of Ni, where the surface Fermi level was found to be 2.58 eV above the valence band edge. Because the measured band gap of our films is 3.23 eV, this places the surface Fermi level at $E_{FS} = E_C - 0.66$ eV. The Fermi level of the bulk was calculated to be $E_F = E_C - 0.16$ eV, giving us a band bending of 0.5 eV. The work functions of the films were determined through the secondary electron tail of the UPS spectra, also referenced to Ni. The work function determined this way gives a value of 5.4 eV for the untreated films.

Surface work function changes of the thin films with various treatment times are shown in Figure 11. The work function changes were obtained through the secondary electron tail of their UPS spectra. The result shows a decrease in surface work function with increasing treatment times, implying a relaxation of band bending at the film surface.

Oxygen Plasma Species. Oxygen plasma was employed to change the surface properties of the TiO_2 thin films. Care was taken to set up a bias in order to inhibit the action of energetic positive ions which could damage the film surface. A typical plasma consists of an equal number of positively and negatively charged species such as ions and electrons, together with a number of uncharged species such as neutrals and radicals. In a radio frequency generated capacitively coupled (RFCC) oxygen plasma, the dominant positive species is the O^{2+} ion and the dominant negative species is the O^- ion. The O^{2+} and O^- ions have a concentration of about 5×10^{15} and 4×10^{15} m^{-3}, respectively, while the electron density is about 1×10^{15} m^{-3}. Among the radical species, atomic oxygen and ozone are present in the same amount at low pressures (<120 mTorr) but the O/O_3 ratio increases beyond that.[50] In particular, it was found that atomic oxygen can be found in significant concentration (∼10^{18} m^{-3}) in the cathodic sheath region and plateauing above the sheath.[51]

DOI: 10.1021/acs.jpcc.5b09272
J. Phys. Chem. C 2015, 119, 27060−27071

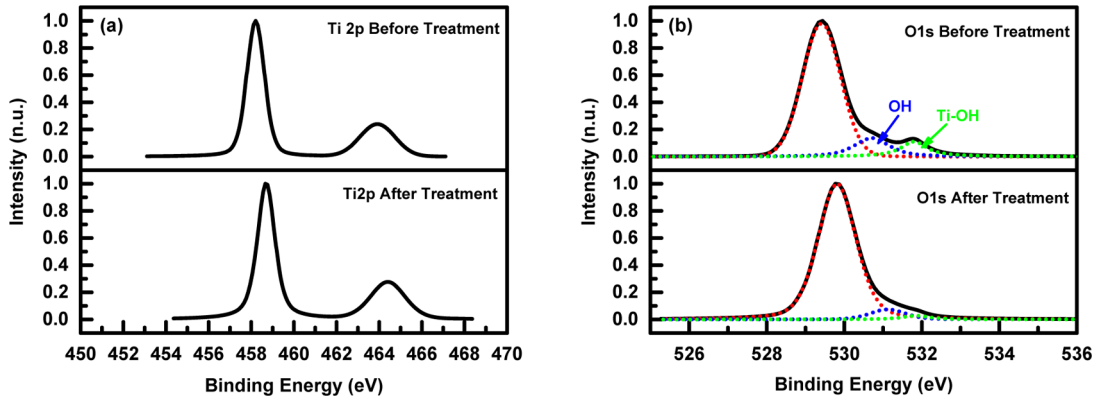

Figure 8. (a) Ti 2p XPS peaks before and after surface treatment. Peak synthesis of the peaks before and after treatment does not suggest the presence of a significant amount of suboxide material, indicating a low defect density in the original film. (b) O 1s XPS peaks before and after surface treatment. Peak synthesis reveals the presence of OH and Ti−OH species[46,47] on the surface of the film. Both species fall in magnitude after surface treatment. The decrease of OH species is consistent with the decrease in the density of surface defects, which have been identified as the active sites for water dissociation.

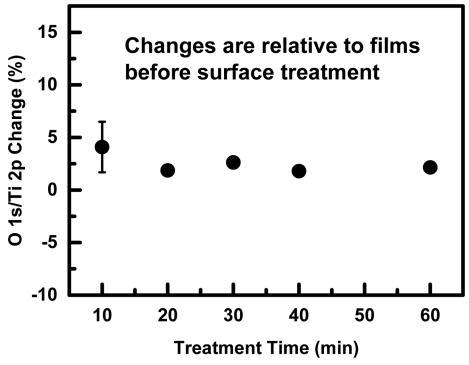

Figure 9. Change in O-to-Ti ratio before and after surface treatment plotted against treatment time. O-to-Ti ratio was obtained from XPS data.

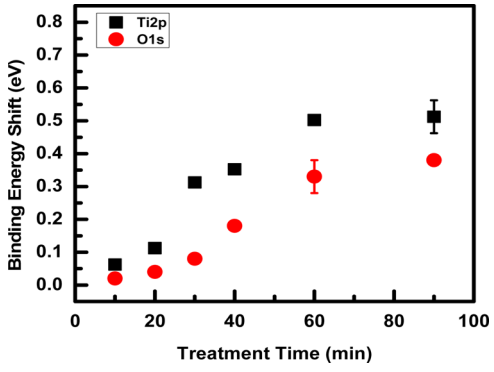

Figure 10. Binding energy shifts of the XPS O 1s and Ti 2p peaks plotted against surface treatment time. Both peaks shifted to higher binding energy level, although the Ti 2p peaks shifted consistently more so than the O 1s peaks. The concomitant peak shift to higher binding energy of the O 1s and Ti 2p peaks points to a relaxation of the band bending near the surface.

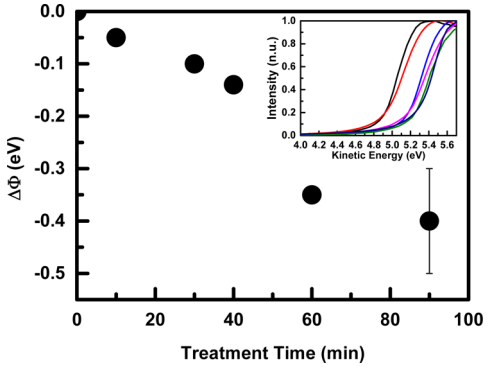

Figure 11. Change in work function of the thin-film surface with treatment time. With longer treatment times, the work function of the film surface decreases. This result is consistent with observations of O 1s and Ti 2p XPS peak shifting toward higher binding energy, together with a decreasing surface state density due to surface oxidation from the remote oxygen plasma treatment. The inset shows the secondary electron tail of the UPS spectra.

In a typical RFCC plasma, the frequency used is 13.56 MHz which the electrons respond to but the ions do not because of their masses. The high mobility of the electrons causes a DC self-bias to develop after the first AC cycle. The electrodes experience a high electron current in the first few cycles and become negatively charged with respect to the plasma, resulting in the formation of an ion sheath around each electrode. The potential gradient set up within the sheath contains the negatively charged ions within the bulk plasma while allowing positive ions to diffuse into the sheath and accelerate toward the target placed on the cathode.[52] As such, negative ions play a minimal role in surface treatment. A screen mesh could be set up over the target to tune the acceleration profile of the impinging ions. A positive bias can be used to decelerate and repel the positive ions from bombarding the surface while allowing neutral radicals to diffuse onto the target surface for reactions.[53] In a similar vein, a negative bias can be used to accelerate the positive ions to enhance surface bombardment.[54] In applications where "gentle" surface reactions are desired without damaging the surface through energetic bombardment, the plasma used is obtained at elevated pressures (100−1000 mTorr)[55] where the reactant supply is high and the ion energy low. To this end, we employed our plasma treatment at an RF power of 50 W and O_2 pressure of 100 Pa. The sheath voltage is about 100 V, so a bias of a decade higher was employed to prevent energetic ions from bombarding the film surface.

DOI: 10.1021/acs.jpcc.5b09272
J. Phys. Chem. C 2015, 119, 27060−27071

DISCUSSION

Surface Oxidation and Band Bending. To assess the effectiveness of the surface treatment, XPS was employed to detect changes before and after the surface modification. The Ti 2p peaks before and after treatment present little difference in terms of their peak shape and suggests that the starting material had a low defect density to begin with. The change in defect density, however, could be evaluated based on the binding energy shift of the XPS peaks.

From XPS data, both the Ti 2p and O 1s peaks presented a shift of up to ∼0.4 eV to higher binding energy after surface treatment, as shown in Figure 10. Figure 12 plots the relative shift in the XPS peak position of Ti 2p and O 1s with treatment time. This relative shift indicates a chemical shift due to surface oxidation from the surface treatment, with the Ti 2p peaks shifting to higher binding energy and O 1s peaks shifting to lower binding energy. This picture is in line with Ti acquiring a higher oxidation state (3+ → 4+) and oxygen filling vacancies on the surface or in the near-surface bulk (visible to XPS), pointing to a slightly more oxidized surface after treatment. The magnitude of the relative shift stabilizes at ∼0.1 eV after 30 min of treatment, suggesting that the effect of remote oxygen plasma on surface oxidation diminishes markedly with longer exposure. The band-bending relaxation achieved this way is up to 0.4 eV, ∼80% of the original value.

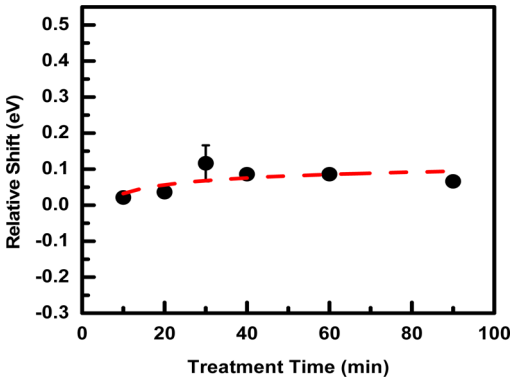

Figure 12. Relative shift between O 1s and Ti 2p plotted against treatment time with the magnitude calculated from the difference in binding energy shift for the same treatment time. The relative shift attains a value of ∼0.1 eV with prolonged treatment time (>30 min), suggesting that the effect of the surface treatment on the surface oxidation state plateaus quickly with longer exposure. The line is drawn to aid the eye.

Further evidence of surface oxidation was provided through an analysis of the amount of OH species detected on the film surface through comparing the O 1s spectra before and after surface treatment. The presence of hydrogen at the film surface is most likely derived from the dissociation of adsorbed water. The presence of surface oxygen vacancies plays an important role in the chemisorption of water through the preferential acceptance of the oxygen in the water molecule. Mentery et al. reported that the dissociative adsorption of water is favored by the presence of surface oxygen vacancies, leading to two types of surface OH groups: (1) those belonging to the incorporated oxygen ion and (2) those attached to a nearby bridging oxygen site.[56,57] Water dissociates readily on the stoichiometric surface of anatase TiO_2,[58] with a coverage approximately 5 times that of molecular water at room temperature on the anatase (101) surface.[59] The adsorption site of water was found to be the 5-fold coordinated Ti sites, Ti(5). Molecular water adsorbs on Ti(5) to form Ti−OH, while the dissociated H^+ bonds with a bridging O to form a bridging hydroxyl − OH (br).[60−62] The presence of oxygen vacancies near the surface has been shown to facilitate and promote the dissociation of molecular water to its hydroxyl fragments.[60,63,64] These oxygen vacancies, predominantly found at subsurface sites in anatase (101),[65] have been cited as being responsible for promoting many surface reactions such as water splitting, CO adsorption, etc. by acting as active sites for the reactants.[63,66−71]

Calculations from the literature using density functional theory indicate that it is unlikely for the oxygen vacancies in the subsurface of anatase to diffuse up to the surface,[72] meaning that a likely explanation for these subsurface defects affecting photocatalysis could be due to their proximity to the surface, acting as a contributor to interfacial charge exchange. The calculations also show that these vacancies tend to stabilize at the first subsurface layer, indicating their ionic radii could very well overlap the surface and affect charge transfer to adsorbates. Figure 13a,b shows a consistent decrease in the OH species across all lengths of surface treatment time. This fall in intensity of the OH species on the film surface after plasma treatment can thus be indicative of a decrease in the density of these surface and near-surface defects post treatment. While the SEM micrographs in Figure 6 suggest that the relative proportion of

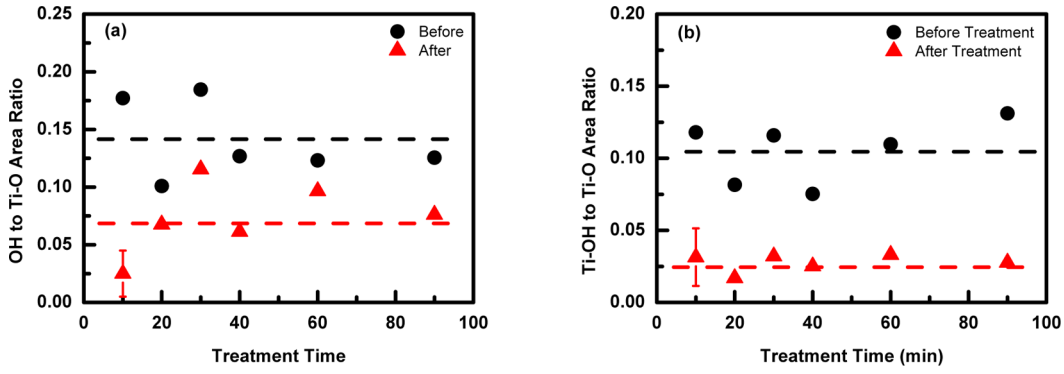

Figure 13. (a) Comparison of the bridging OH to Ti−O area ratio and (b) Ti−OH to Ti−O area ratio from O 1s XPS peaks across six treated samples. The samples were treated with increasing lengths of time, starting with 10 min for the first sample, followed by 20, 30, 40, 60, and 90 min for the successive samples. It is evident that OH species dropped significantly after surface treatment. This can be attributed to a decrease in the density of oxygen vacancies.[66,78]

DOI: 10.1021/acs.jpcc.5b09272
J. Phys. Chem. C 2015, 119, 27060−27071

anatase facets does not change after plasma treatment, the decrease in OH species in our result after plasma treatment can suggest a differential change in O vacancy concentration from different facets, such as (101) and (001). Li et al. concluded that the majority anatase (101) surface was hydrophobic, while the minority (001) surface was terminated by dissociated water molecules.[73] (001) facets have been suggested to be the most active sites theoretically,[74−76] and some experimental confirmation has accumulated.[77] The decrease observed here in surface OH species could indicate the preferential oxidation of (001) facets after plasma treatment, resulting in a drop in reactivity observed in our study. It is worth noting that both rate measurements and V_S average spatially over all exposed facets and that even if there were differential changes to O vacancies among the facets, the model would be able to capture it meaningfully through V_S.

We postulate that this change in surface defect density affects photocatalytic rate only indirectly through a change in surface potential, and not directly via some atomic scale reaction. In addition, the change in surface potential/photoactivity of the photocatalyst seems to be robust against air and water exposure, retaining the same photocatalytic rates after multiple degradation runs. We believe that this robustness results from the character of oxygen vacancies, where they form preferentially near the surface of anatase TiO_2.[65]

More evidence of mild surface oxidation is given by comparing the O and Ti ratio before and after surface treatment. Figure 9 shows the change in O/Ti ratio after treatment, presenting an increase in the O/Ti ratio, albeit of a modest average value of 2.5% ± 1. This slight increase can be construed as mild surface oxidation of the film surface with no contribution from suboxides (usually requiring changes of >10%), in contrast with a heavily defected surface where suboxide XPS peaks, such as those of Ti_2O_3 and TiO, could be readily identified.[37]

It is worth noting that while the plasma removed O vacancies from the material surface, negatively charged ions can exist in the plasma. The electrically biased screen would have actually augmented implantation of such ions into the surface. Although such implantation could have helped to eliminate O vacancies, it could have also induced various kinds of lattice damage whose effects on V_S are unknown. Indeed, observations of band relaxation in response to such implantation have been reported on Si and GaAs.[79]

Note that surface oxidation can change the number of active sites that mediate photocatalysis. On TiO_2 surfaces, oxygen vacancies and/or under-coordinated Ti cations are the active sites for most organic molecules, and changes in the concentration of these sites, rather than the width of the SCL, could conceivably cause some of the change in reactivity. The present paper shows that the model accurately predicts the direction, magnitude, and functional form of the rate change with respect to V_S. Assuming that the number of active sites do change after plasma treatment, the effects would act to change the Fermi level of the surface, which directly affects the value of V_S. Our previous work[8] shows that the photocurrent model accurately predicts the direction, magnitude, and functional form of the relationship between rates and N_d. The model also predicts and constrains the way rates should vary with an entirely different parameter, V_S. Both N_d and V_S act by affecting the width of the space charge layer, although in different and independent ways. The results of the present work accord with both the predictions and constraints imposed by that physical picture in terms of the direction, magnitude, and functional form of the rate versus V_S. If the number of active sites does change after plasma treatment, the effects would act in addition to those that necessarily follow from changes in V_S. Because we do not observe significant deviation from the prediction based upon V_S, the effects from active site concentration are constrained to be rather small.

Surface treatment did not significantly change the adsorption of MB on the film surface, as shown by the absorbance of MB on the films before and after treatment, shown in Figure 14.

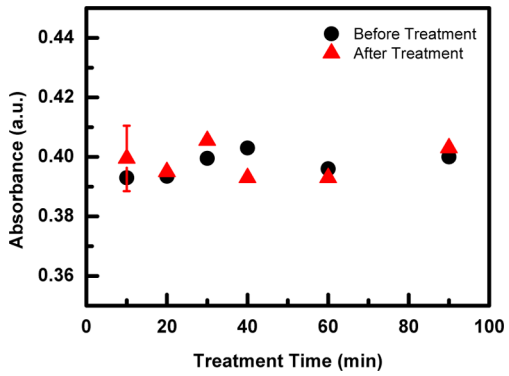

Figure 14. MB absorbance with treatment time, before and after surface treatment. The lack of a trend indicates that adsorption of MB on the films did not vary significantly with treatment time.

The average absorbances before and after surface treatment were both 0.398 ± 0.011. MB in solution is a cationic dye which adsorbs onto the surface of TiO_2 through Coulombic interaction with Ti−O through its cationic functional group.[20] This is evidenced by the influence of solution pH on the amount of MB adsorbed, which affects the surface charge of TiO_2. Relative to the point-of-zero-charge of TiO_2 (pH ~6.3),[80,81] a more acidic solution causes the surface to be more positive while a more alkaline solution causes it to be more negative, described by the ionization state of the surface:

$$TiOH + H^+ \Leftrightarrow TiOH_2^+ \quad (6)$$

$$TiOH + OH^+ \Leftrightarrow TiO^- \quad (7)$$

It is not surprising then that surface treatment of the films did not affect MB adsorption significantly in solution, because solution pH plays the significant role. The insensitivity of MB adsorption to surface treatment implies that at the very least, MB supply at the anatase surface is not responsible for any change in MB degradation rate.

Rate changes caused by the accumulation of surface carbon species are also unlikely because the use of oxygen plasma treatment for surface cleaning is well-documented[36,82,83] and degradation rates actually decreased after surface treatment. Contributions from carbonaceous species before and after treatment (Figure 15a,b) reveal no significant changes to the carbon content that could explain the fall in rates after treatment. All these suggest that surface carbon played no part in affecting the rate of MB degradation.

Band Bending Determination via Work Function. Work function measurements from UPS showed shifts in work function values consistent with the binding energy shifts of Ti 2p and O 1s from XPS. The work function of a surface is defined as the energy required to remove an electron from the Fermi level in a material, then it put at rest at an infinite

DOI: 10.1021/acs.jpcc.5b09272
J. Phys. Chem. C 2015, 119, 27060−27071

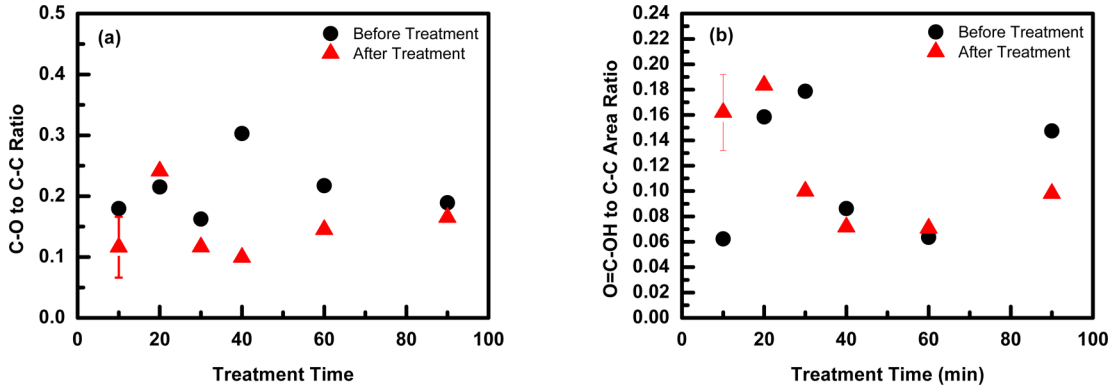

Figure 15. (a) C−O to graphitic carbon area ratio and (b) O═C−OH to graphitic carbon area ratio across six samples. No significant changes in the ratios could be perceived before and after surface treatment. It seems that remote oxygen plasma treatment does little to alter the presence of such carbon species. As such, we attribute changes in photoactivity to causes other than the relative amount of such species on the catalyst surface.

distance away from the material (usually tens to hundreds of angstroms would suffice). Its value is therefore indicative of the charge-transfer properties near the surface. The work function of oxide semiconductors involves the following components:[84]

$$\Phi_S = \mu + \Phi_{BB} + \chi \tag{8}$$

where Φ_S is the surface work function, μ the chemical potential, Φ_{BB} the degree of band bending, and χ the electron affinity. This relationship is presented in Figure 16. For oxidation and

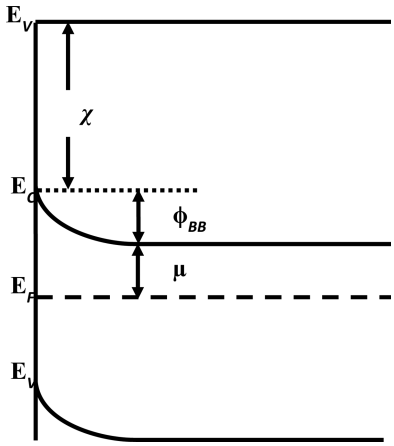

Figure 16. Band model representing the components which make up the work function of an oxide semiconductor.

reduction of oxide semiconductors within a single phase regime, changes in the work function are determined by the chemical potential and the degree of band bending while the electron affinity remains constant, giving us

$$\Delta\Phi_S = \mu + \Delta\Phi_{BB} \tag{9}$$

At room temperature, work function change is due mainly to the band-bending component, while the change in chemical potential is negligibly small.[85] As such, we can attribute the change in work function for our thin films after surface treatment to a relaxation in band bending:

$$\Delta\Phi_S = \Delta\Phi_{BB} \tag{10}$$

The work function change from UPS and the binding energy change in XPS both give a value of ∼0.4 eV. This is consistent with a decrease in O vacancies after surface treatment as the density of surface states correlates positively with the degree of band bending,[86] whereas for charge equilibrium to occur between the surface and the bulk, less charge transfer is required, resulting in a smaller SCL.

Correspondence of Photocatalytic Rates with Model. A comparison between the changes in initial rate of MB degradation with the model prediction as embodied in eq 2 shows good correspondence, as shown in Figure 17. There are

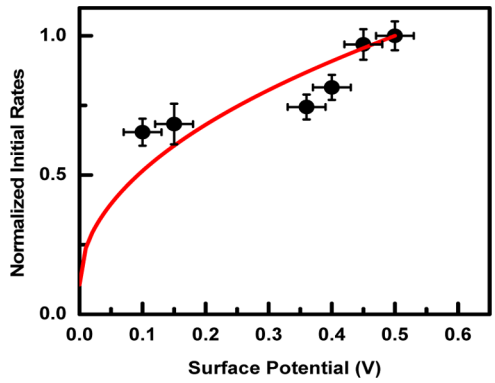

Figure 17. Comparison between change in initial rate of MB degradation and the change in the photocurrent from the model. The surface potential for the untreated surface (the point furthest to the right) was measured to be 0.5 eV. Horizontal and vertical errors are standard errors of coefficient from regression analysis.

no adjustable parameters in the photocurrent model—the parameters were either measured or estimated. With longer surface treatment times, the rate of MB degradation falls accordingly up to about 35% from before the treatment. Because the primary pathway by which MB is degraded is through oxidation,[19] our results suggest a diminished ability at the surface to oxidize and degrade MB. This direction of change predicted by the photocurrent model implies a relaxation of the surface band bending caused by a decrease in magnitude of the surface potential. In the present system, we calculate our quantum yield, QY, by considering the initial number of MB molecules degraded per unit time versus the number of holes promoted to the surface per unit time, according to the following equation:

$$\mathrm{QY} = \frac{r_0}{J_{PC}} \tag{11}$$

DOI: 10.1021/acs.jpcc.5b09272
J. Phys. Chem. C 2015, 119, 27060−27071

where r_0 is the initial rate. These calculations yield a value of 0.15% ± 0.02% for QY, in line with those reported in the literature. Houas et al.[20] reported values of 0.12% and 0.14% for 290 and 340 nm light, respectively, for his study on MB degradation, and Matthews reported a value close to 0.1%.[24]

CONCLUSION

The importance of defect engineering in TiO_2 photocatalysis has been recognized for several years,[87] although the early focus was on the concentration of point defects within crystallites. Similarly, the importance of band bending for photocatalysis had been recognized,[88,89] although the interest has gravitated toward metal−semiconductor contacts and other methods of band control. The coordinated use of multiple defect engineering practices to control the concentration and spatial distribution of charged defects in polycrystalline material, for the specific purpose of quantitative manipulation of band bending, does not appear to have been articulated or demonstrated as in the present work. Here, film thickness provides a control pathway[8] for N_D through (incompletely understood) effects of medium range atomic ordering in the early stages of film synthesis,[17] while remote oxygen plasma treatment of the polycrystalline surface provides removal of oxygen vacancies from the near-surface region to control V_S. These twin effects act largely independently to vary the width of the SCL, which in turn affects the proportion of photocarriers that are swept to the surface to induce photochemistry. Such principles should work well for thin-film photocatalysts operating in gases or liquids of low ionic strength. In liquids of high ionic strength, it may prove more difficult to maintain control of surface potential via near-surface defects, as the effects of redox couples within the solution may prevail. These concepts must also be modified for isolated photocatalyst particles whose width is sufficiently small to put the particle center within the nominal width of the SCL, in which case the particle has insufficient bulk to screen its opposing sides from each other (affecting V_S), imposing a hard constraint on the maximum width of the SCL from which particles can be swept. Future work should focus on widening the window of accessible values for N_D and V_S, as well as determining the extent to which extrinsic dopants augment or inhibit the effects of native defects examined here.

AUTHOR INFORMATION

Corresponding Author

*E-mail: eseebaue@illinois.edu. Phone: (217) 244-9214.

Notes

The authors declare no competing financial interest.

ACKNOWLEDGMENTS

This work was supported by NSF (DMR 10-05720 and 13-06822) and Singapore's Agency for Science, Technology and Research.

REFERENCES

(1) Fujishima, A.; Hashimoto, K.; Watanabe, T. *TiO_2 Photocatalysis: Fundamentals and Applications*; BKC: Tokyo, 1999.

(2) Paz, Y.; Luo, Z.; Rabenberg, L.; Heller, A. Photooxidative Self-Cleaning Transparent Titanium Dioxide Films on Glass. *J. Mater. Res.* **1995**, *10*, 2842−2848.

(3) Chung, C. J.; Lin, H. I.; Tsou, H. K.; Shi, Z. Y.; He, J. L. An Antimicrobial TiO_2 Coating for Reducing Hospital-Acquired Infection. *J. Biomed. Mater. Res., Part B* **2008**, *85B*, 220−224.

(4) Fu, G.; Vary, P. S.; Lin, C.-T. *J. Phys. Chem. B* **2005**, *109*, 8889−8898.

(5) Wang, Y.; Wang, L. L.; Liu, M. Y. Antifouling and Enhancing Pool Boiling by TiO_2 Coating Surface in Nanometer Scale Thickness. *AIChE J.* **2007**, *53*, 3062−3076.

(6) Kim, S. H.; Kwak, S.-Y.; Sohn, B.-H.; Park, T. H. Design of TiO_2 Nanoparticle Self-Assembled Aromatic Polyamide Thin-Film-Composite (TFC) Membrane as an Approach to Solve Biofouling Problem. *J. Membr. Sci.* **2003**, *211*, 157−165.

(7) Takahashi, M.; Tsukigi, K.; Uchino, T.; Yoko, T. Enhanced Photocurrent in Thin Film TiO_2 Electrodes Prepared by Sol−Gel Method. *Thin Solid Films* **2001**, *388*, 231−236.

(8) Ong, S. W. D.; Lin, J.; Seebauer, E. G. Control of Methylene Blue Photo-Oxidation Rate over Polycrystalline Anatase TiO_2 Thin Films via Carrier Concentration. *J. Phys. Chem. C* **2015**, *119*, 11662−11671.

(9) Seebauer, E. G.; Noh, K. W. Trends in Semiconductor Defect Engineering at the Nanoscale. *Mater. Sci. Eng., R* **2010**, *70*, 151−168.

(10) Dev, K.; Jung, M. Y. L.; Gunawan, R.; Braatz, R. D.; Seebauer, E. G. Mechanism for Coupling Between Properties of Interfaces and Bulk Semiconductors. *Phys. Rev. B: Condens. Matter Mater. Phys.* **2003**, *68*, 195311.

(11) Dev, K.; Seebauer, E. G. Band Bending at the Si(111)−SiO_2 Interface Induced by Low-Energy Ion Bombardment. *Surf. Sci.* **2004**, *550*, 185−191.

(12) Kondratenko, Y.; Seebauer, E. G. Interface-Mediated Photostimulation Effects on Diffusion and Activation of Boron Implanted into Silicon. *ECS J. Solid State Sci. Technol.* **2013**, *2*, P235−P242.

(13) Sellers, M. C. K.; Seebauer, E. G. Manipulation of Polycrystalline TiO_2 Carrier Concentration via Electrically Active Native Defects. *J. Vac. Sci. Technol., A* **2011**, *29*, 061503.

(14) Seebauer, E. G.; Kratzer, M. C. Charged Point Defects in Semiconductors. *Mater. Sci. Eng., R* **2006**, *55*, 57−149.

(15) Seebauer, E. G.; Kratzer, M. C. *Charged Semiconductor Defects: Structure, Thermodynamics and Diffusion*; Springer: London, 2009.

(16) Sellers, M. C. K.; Seebauer, E. G. Measurement Method for Carrier Concentration in TiO_2 via the Mott−Schottky Approach. *Thin Solid Films* **2011**, *519*, 2103−2110.

(17) Eitan Barlaz, D.; Seebauer, E. G. Manipulation of Carrier Concentration, Crystallite Size and Density in Polycrystalline Anatase TiO_2 via Amorphous-Phase Medium Range Atomic Order. *CrystEngComm* **2015**, *17*, 2101−2109.

(18) Lakshmi, S.; Renganathan, R.; Fujita, S. Study on TiO_2-Mediated Photocatalytic Degradation of Methylene Blue. *J. Photochem. Photobiol., A* **1995**, *88*, 163−167.

(19) Zhang, T.; Oyama, T.; Aoshima, A.; Hidaka, H.; Zhao, J.; Serpone, N. Photooxidative N-Demethylation of Methylene Blue in Aqueous TiO_2 Dispersions under UV Irradiation. *J. Photochem. Photobiol., A* **2001**, *140*, 163−172.

(20) Houas, A.; Lachheb, H.; Ksibi, M.; Elaloui, E.; Guillard, C.; Herrmann, J.-M. Photocatalytic Degradation Pathway of Methylene Blue in Water. *Appl. Catal., B* **2001**, *31*, 145−157.

(21) Kapinus, E.; Viktorova, T. Kinetics of the Photocatalytic Degradation of Methylene Blue on Titanium Dioxide. *Theor. Exp. Chem.* **2010**, *46*, 163−167.

(22) Kuo, W. S.; Ho, P. H. Solar Photocatalytic Decolorization of Methylene Blue in Water. *Chemosphere* **2001**, *45*, 77−83.

(23) Ling, C. M.; Mohamed, A. R.; Bhatia, S. Performance of Photocatalytic Reactors Using Immobilized TiO_2 Film for the Degradation of Phenol and Methylene Blue Dye Present in Water Stream. *Chemosphere* **2004**, *57*, 547−554.

(24) Matthews, R. W. Photocatalytic Oxidation and Adsorption of Methylene Blue on Thin Films of Near-Ultraviolet-Illuminated TiO_2. *J. Chem. Soc., Faraday Trans. 1* **1989**, *85*, 1291−1302.

(25) Mills, A. An Overview of the Methylene Blue ISO Test for Assessing the Activities of Photocatalytic Films. *Appl. Catal., B* **2012**, *128*, 144−149.

(26) Tennakone, K.; Senadeera, S.; Priyadharshana, A. TiO_2 Catalysed Photo-Oxidation of Water in the Presence of Methylene Blue. *Sol. Energy Mater. Sol. Cells* **1993**, *29*, 109−113.

DOI: 10.1021/acs.jpcc.5b09272
J. Phys. Chem. C 2015, 119, 27060−27071

(27) Yu, Z.; Chuang, S. S. C. Probing Methylene Blue Photocatalytic Degradation by Adsorbed Ethanol with In Situ IR. *J. Phys. Chem. C* **2007**, *111*, 13813−13820.
(28) Wu, C.-H.; Chern, J.-M. Kinetics of Photocatalytic Decomposition of Methylene Blue. *Ind. Eng. Chem. Res.* **2006**, *45*, 6450−6457.
(29) Henrich, V. E.; Cox, P. A. *The Surface Science of Metal Oxides*; Cambridge University Press: New York, 1994.
(30) Butler, M. A. Photoelectrolysis and Physical Properties of the Semiconducting Electrode WO_2. *J. Appl. Phys. (Melville, NY, U. S.)* **1977**, *48*, 1914−1920.
(31) Rothenberger, G.; Moser, J.; Graetzel, M.; Serpone, N.; Sharma, D. K. Charge Carrier Trapping and Recombination Dynamics in Small Semiconductor Particles. *J. Am. Chem. Soc.* **1985**, *107*, 8054−8059.
(32) Yamada, Y.; Kanemitsu, Y. Determination of Electron and Hole Lifetimes of Rutile and Anatase TiO_2 Single Crystals. *Appl. Phys. Lett.* **2012**, *101*, 133907.
(33) Wilson, J. N.; Idriss, H. Structure Sensitivity and Photocatalytic Reactions of Semiconductors. Effect of the Last Layer Atomic Arrangement. *J. Am. Chem. Soc.* **2002**, *124*, 11284−11285.
(34) Epling, G. A.; Lin, C. Photoassisted Bleaching of Dyes Utilizing TiO_2 and Visible Light. *Chemosphere* **2002**, *46*, 561−570.
(35) Godyak, V. A.; Piejak, R. B.; Alexandrovich, B. M. Electrical Characteristics of Parallel-Plate RF Discharges in Argon. *IEEE Trans. Plasma Sci.* **1991**, *19*, 660−676.
(36) Oehrlein, G. S.; Scilla, G. J.; Jeng, S.-J. Efficiency of Oxygen Plasma Cleaning of Reactive Ion Damaged Silicon Surfaces. *Appl. Phys. Lett.* **1988**, *52*, 907−909.
(37) Kim, Y.; Yoo, B. J.; Vittal, R.; Lee, Y.; Park, N.-G.; Kim, K.-J. Low-Temperature Oxygen Plasma Treatment of TiO_2 Film For Enhanced Performance of Dye-Sensitized Solar Cells. *J. Power Sources* **2008**, *175*, 914−919.
(38) Wu, W.-Y.; Shih, T.-W.; Chen, P.; Ting, J.-M.; Chen, J.-M. Plasma Surface Treatments of TiO_2 Photoelectrodes for Use in Dye-Sensitized Solar Cells. *J. Electrochem. Soc.* **2011**, *158*, K101−K106.
(39) Shih, W. S.; Young, S. J.; Ji, L. W.; Water, W.; Meen, T. H.; Shiu, H. W. Effect of Oxygen Plasma Treatment on Characteristics of TiO_2 Photodetectors. *IEEE Sens. J.* **2011**, *11*, 3031−3035.
(40) Takeuchi, K.; Nakamura, I.; Matsumoto, O.; Sugihara, S.; Ando, M.; Ihara, T. Preparation of Visible-Light-Responsive Titanium Oxide Photocatalysts by Plasma Treatment. *Chem. Lett.* **2000**, *29*, 1354−1355.
(41) Bockris, J. O. M.; Reddy, A. K. N.; Gamboa-Aldeco, M. E. *Modern Electrochemistry 2A: Fundamentals of Electrodics*; Springer US: Boston, 2002.
(42) Dillon, E. P.; Crouse, C. A.; Barron, A. R. Synthesis, Characterization, and Carbon Dioxide Adsorption of Covalently Attached Polyethyleneimine-Functionalized Single-Wall Carbon Nanotubes. *ACS Nano* **2008**, *2*, 156−164.
(43) Gogotsi, Y. G.; Uvarova, I. V. *Nanostructured Materials and Coatings in Biomedical and Sensor*; Springer Netherlands: Dordrecht, 2003.
(44) Liang, F.; Beach, J. M.; Rai, P. K.; Guo, W.; Hauge, R. H.; Pasquali, M.; Smalley, R. E.; Billups, W. E. Highly Exfoliated Water-Soluble Single-Walled Carbon Nanotubes. *Chem. Mater.* **2006**, *18*, 1520−1524.
(45) Yang, C.-M.; Kanoh, H.; Kaneko, K.; Yudasaka, M.; Iijima, S. Adsorption Behaviors of HiPco Single-Walled Carbon Nanotube Aggregates for Alcohol Vapors. *J. Phys. Chem. B* **2002**, *106*, 8994−8999.
(46) Sham, T. K.; Lazarus, M. S. X-Ray Photoelectron Spectroscopy (XPS) Studies of Clean and Hydrated TiO_2 (Rutile) Surfaces. *Chem. Phys. Lett.* **1979**, *68*, 426−432.
(47) Wang, L. Q.; Baer, D. R.; Engelhard, M. H.; Shultz, A. N. The Adsorption of Liquid and Vapor Water on TiO_2 (110) Surfaces: The Role of Defects. *Surf. Sci.* **1995**, *344*, 237−250.
(48) Erdem, B.; Hunsicker, R. A.; Simmons, G. W.; Sudol, E. D.; Dimonie, V. L.; El-Aasser, M. S. XPS and FTIR Surface Characterization of TiO_2 Particles Used in Polymer Encapsulation. *Langmuir* **2001**, *17*, 2664−2669.
(49) Jensen, H.; Soloviev, A.; Li, Z.; Søgaard, E. G. XPS and FTIR Investigation of the Surface Properties of Different Prepared Titania Nano-Powders. *Appl. Surf. Sci.* **2005**, *246*, 239−249.
(50) Stoffels, E.; Stoffels, W. W.; Vender, D.; Kando, M.; Kroesen, G. M. W.; de Hoog, F. J. Negative Ions in a Radio-Frequency Oxygen Plasma. *Phys. Rev. E: Stat. Phys., Plasmas, Fluids, Relat. Interdiscip. Top.* **1995**, *51*, 2425−2435.
(51) Selwyn, G. S. Spatially Resolved Detection of O Atoms in Etching Plasmas by Two-photon Laser-Induced Fluorescence. *J. Appl. Phys. (Melville, NY, U. S.)* **1986**, *60*, 2771−2774.
(52) Schüngel, E.; Zhang, Q. Z.; Iwashita, S.; Schulze, J.; Hou, L. J.; Wang, Y. N.; Czarnetzki, U. Control of Plasma Properties in Capacitively Coupled Oxygen Discharges via the Electrical Asymmetry Effect. *J. Phys. D: Appl. Phys.* **2011**, *44*, 285205.
(53) Mittal, K. L. *Surface and Colloid Science in Computer Technology*; Springer US: New York, 1987.
(54) Pei, Y.; Xie, D.; Leng, Y.; Qian, L.; Sun, H.; Huang, N. Effects of Screen-Grid Bias Voltage on the Microstructure and Properties of the Ultrahigh Molecular Weight Polyethylene (UHMWPE) Modified by Oxygen Plasma. *Vacuum* **2012**, *86*, 1945−1951.
(55) Hartney, M. A.; Hess, D. W.; Soane, D. S. Oxygen Plasma Etching for Resist Stripping and Multilayer Lithography. *J. Vac. Sci. Technol., B: Microelectron. Process. Phenom.* **1989**, *7*, 1−13.
(56) Menetrey, M.; Markovits, A.; Minot, C. Reactivity of a Reduced Metal Oxide Surface: Hydrogen, Water and Carbon Monoxide Adsorption on Oxygen Defective Rutile TiO_2. *Surf. Sci.* **2003**, *524*, 49−62.
(57) Calatayud, M.; Markovits, A.; Menetrey, M.; Mguig, B.; Minot, C. Adsorption on Perfect and Reduced Surfaces of Metal Oxides. *Catal. Today* **2003**, *85*, 125−143.
(58) Walle, L. E.; Borg, A.; Uvdal, P.; Sandell, A. Experimental Evidence for Mixed Dissociative and Molecular Adsorption of Water on a Rutile TiO_2 (110) Surface Without Oxygen Vacancies. *Phys. Rev. B: Condens. Matter Mater. Phys.* **2009**, *80*, 235436.
(59) Walle, L. E.; Borg, A.; Johansson, E. M. J.; Plogmaker, S.; Rensmo, H.; Uvdal, P.; Sandell, A. Mixed Dissociative and Molecular Water Adsorption on Anatase TiO_2 (101). *J. Phys. Chem. C* **2011**, *115*, 9545−9550.
(60) Aschauer, U.; He, Y.; Cheng, H.; Li, S.-C.; Diebold, U.; Selloni, A. Influence of Subsurface Defects on the Surface Reactivity of TiO_2: Water on Anatase (101). *J. Phys. Chem. C* **2010**, *114*, 1278−1284.
(61) Lindan, P. J. D.; Zhang, C. Exothermic Water Dissociation on the Rutile TiO_2 (110) Surface. *Phys. Rev. B: Condens. Matter Mater. Phys.* **2005**, *72*, 075439.
(62) Wendt, S.; Matthiesen, J.; Schaub, R.; Vestergaard, E. K.; Lægsgaard, E.; Besenbacher, F.; Hammer, B. Formation and Splitting of Paired Hydroxyl Groups on Reduced TiO_2 (110). *Phys. Rev. Lett.* **2006**, *96*, 066107.
(63) Bikondoa, O.; Pang, C. L.; Ithnin, R.; Muryn, C. A.; Onishi, H.; Thornton, G. Direct Visualization of Defect-Mediated Dissociation of Water on TiO_2 (110). *Nat. Mater.* **2006**, *5*, 189−192.
(64) Tilocca, A.; Selloni, A. Reaction Pathway and Free Energy Barrier for Defect-Induced Water Dissociation on the (101) surface of TiO_2 - Anatase. *J. Chem. Phys.* **2003**, *119*, 7445−7450.
(65) He, Y.; Dulub, O.; Cheng, H.; Selloni, A.; Diebold, U. Evidence for the Predominance of Subsurface Defects on Reduced Anatase TiO_2 (101). *Phys. Rev. Lett.* **2009**, *102*, 106105.
(66) Schaub, R.; Thostrup, P.; Lopez, N.; Lægsgaard, E.; Stensgaard, I.; Nørskov, J. K.; Besenbacher, F. Oxygen Vacancies as Active Sites for Water Dissociation on Rutile TiO_2 (110). *Phys. Rev. Lett.* **2001**, *87*, 266104.
(67) Wahlström, E.; Lopez, N.; Schaub, R.; Thostrup, P.; Rønnau, A.; Africh, C.; Lægsgaard, E.; Nørskov, J. K.; Besenbacher, F. Bonding of Gold Nanoclusters to Oxygen Vacancies on Rutile TiO_2 (110). *Phys. Rev. Lett.* **2003**, *90*, 026101.
(68) Linsebigler, A.; Lu, G.; Yates, J. J. T. CO Chemisorption on TiO_2 (110): Oxygen Vacancy Site Influence on CO Adsorption. *J. Chem. Phys.* **1995**, *103*, 9438−9443.

DOI: 10.1021/acs.jpcc.5b09272
J. Phys. Chem. C 2015, 119, 27060−27071

(69) Nowotny, J.; Bak, T.; Nowotny, M. K.; Sheppard, L. R. TiO_2 Surface Active Sites for Water Splitting. *J. Phys. Chem. B* **2006**, *110*, 18492−18495.
(70) Lu, G.; Linsebigler, A.; Yates, J. T. Ti^{3+} Defect Sites on TiO_2 (110): Production and Chemical Detection of Active Sites. *J. Phys. Chem.* **1994**, *98*, 11733−11738.
(71) Martinez, U.; Vilhelmsen, L. B.; Kristoffersen, H. H.; Stausholm-Møller, J.; Hammer, B. Steps on Rutile TiO_2 (110): Active Sites for Water and Methanol Dissociation. *Phys. Rev. B: Condens. Matter Mater. Phys.* **2011**, *84*, 205434.
(72) Cheng, H.; Selloni, A. Surface and Subsurface Oxygen Vacancies in Anatase TiO_2 and Differences with Rutile. *Phys. Rev. B: Condens. Matter Mater. Phys.* **2009**, *79*, 092101.
(73) Li, Y.-F.; Liu, Z.-P.; Liu, L.; Gao, W. Mechanism and Activity of Photocatalytic Oxygen Evolution on Titania Anatase in Aqueous Surroundings. *J. Am. Chem. Soc.* **2010**, *132*, 13008−13015.
(74) Gong, X.-Q.; Selloni, A. Reactivity of Anatase TiO_2 Nanoparticles: The Role of the Minority (001) Surface. *J. Phys. Chem. B* **2005**, *109*, 19560−19562.
(75) Lazzeri, M.; Vittadini, A.; Selloni, A. Structure and Energetics of Stoichiometric TiO_2 Anatase Surfaces. *Phys. Rev. B: Condens. Matter Mater. Phys.* **2001**, *63*, 155409.
(76) Vittadini, A.; Casarin, M.; Selloni, A. Chemistry of and on TiO_2-Anatase Surfaces by DFT Calculations: A Partial Review. *Theor. Chem. Acc.* **2007**, *117*, 663−671.
(77) Wang, Y.; Sun, H.; Tan, S.; Feng, H.; Cheng, Z.; Zhao, J.; Zhao, A.; Wang, B.; Luo, Y.; Yang, J.; Hou, J. G. Role of Point Defects on the Reactivity of Reconstructed Anatase Titanium Dioxide (001) Surface. *Nat. Commun.* **2013**, *4*, 2214.
(78) Pasquariello, D.; Lindeberg, M.; Hedlund, C.; Hjort, K. Surface Energy as a Function of Self-Bias Voltage in Oxygen Plasma Wafer Bonding. *Sens. Actuators, A* **2000**, *82*, 239−244.
(79) Ashok, S. In *Plasma and Ion Beam Process-Induced Damage in Semiconductors: Review and Retrospective*. In Proceedings of 7th International Conference on Solid-State and Integrated Circuits Technology, Oct., 18−21, 2004. DOI: 10.1109/ICSICT.2004.1435063.
(80) Shih, Y.-H.; Liu, W.-S.; Su, Y.-F. Aggregation of Stabilized TiO_2 Nanoparticle Suspensions in the Presence of Inorganic Ions. *Environ. Toxicol. Chem.* **2012**, *31*, 1693−1698.
(81) Chou, J.-C.; Liao, L. P. Study on pH at the Point of Zero Charge of TiO_2 pH Ion-Sensitive Field Effect Transistor Made by the Sputtering Method. *Thin Solid Films* **2005**, *476*, 157−161.
(82) Li, H.; Belkind, A.; Jansen, F.; Orban, Z. An In Situ XPS Study of Oxygen Plasma Cleaning of Aluminum Surfaces. *Surf. Coat. Technol.* **1997**, *92*, 171−177.
(83) O'Kane, D. F.; Mittal, K. L. Plasma Cleaning of Metal Surfaces. *J. Vac. Sci. Technol. (N. Y., NY, U. S.)* **1974**, *11*, 567−569.
(84) Nowotny, J.; Dufour, L. C. *Surface and Near-Surface Chemistry of Oxide Materials*; Elsevier: New York, 1988.
(85) Nowotny, J.; Bak, T.; Sheppard, L. R.; Nowotny, M. K. Reactivity of Titanium Dioxide with Oxygen at Room Temperature and the Related Charge Transfer. *J. Am. Chem. Soc.* **2008**, *130*, 9984−9993.
(86) Kronik, L.; Shapira, Y. Surface Photovoltage Phenomena: Theory, Experiment, and Applications. *Surf. Sci. Rep.* **1999**, *37*, 1−206.
(87) Nowotny, M. K.; Sheppard, L. R.; Bak, T.; Nowotny, J. Defect Chemistry of Titanium Dioxide. Application of Defect Engineering in Processing of TiO_2-Based Photocatalystst. *J. Phys. Chem. C* **2008**, *112*, 5275−5300.
(88) Jing, L.; Sun, X.; Shang, J.; Cai, W.; Xu, Z.; Du, Y.; Fu, H. Review of Surface Photovoltage Spectra of Nano-Sized Semiconductor and its Applications in Heterogeneous Photocatalysis. *Sol. Energy Mater. Sol. Cells* **2003**, *79*, 133−151.
(89) Zhang, Z.; Yates, J. T. Band Bending in Semiconductors: Chemical and Physical Consequences at Surfaces and Interfaces. *Chem. Rev. (Washington, DC, U. S.)* **2012**, *112*, 5520−5551.

DOI: 10.1021/acs.jpcc.5b09272
J. Phys. Chem. C 2015, 119, 27060−27071